Journal of Colloid and Interface Science 606 (2022) 826–836

Contents lists available at ScienceDirect

Journal of Colloid and Interface Science

journal homepage: www.elsevier.com/locate/jcis

Spherical mesoporous Fe-N-C single-atom nanozyme for photothermal and catalytic synergistic antibacterial therapy

Youyou Feng [a], Jing Qin [a], Yu Zhou [b], Qin Yue [b,*], Jing Wei [a,*]

[a] Institute of Analytical Chemistry and Instrument for Life Science, The Key Laboratory of Biomedical Information Engineering of Ministry of Education, School of Life Science and Technology, Xi'an Jiaotong University, Xi'an, Shaanxi 710049, China
[b] Institute of Fundamental and Frontier Science, University of Electronic Science and Technology of China, Chengdu 610054, P. R. China

GRAPHICAL ABSTRACT

Spherical mesoporous Fe-N-C single-atom nanozyme with excellent peroxidase-like activity and photothermal property is developed via a soft-template method. Light irradiation can not only improve the catalytic activity of nanozyme via the increasement of reaction temperature, but also be used to kill bacteria via photothermal treatment. The synergistic effect can effectively accelerate the wound healing *in vivo*.

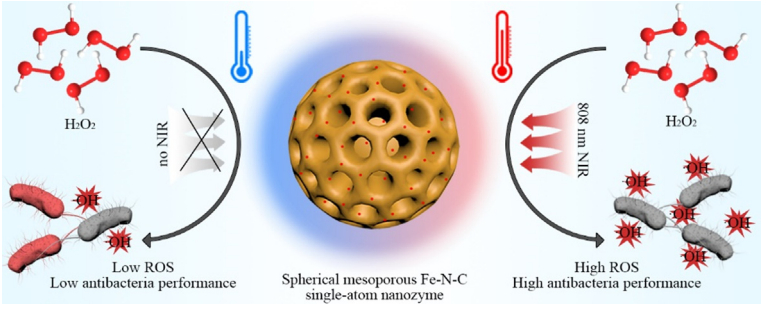

ARTICLE INFO

Article history:
Received 21 June 2021
Revised 22 July 2021
Accepted 7 August 2021
Available online 14 August 2021

Keywords:
Mesoporous material
Single-atom catalyst
Nanozyme
Photothermal treatment
Antibacterial therapy

ABSTRACT

Nanozyme has been regarded as an efficient antibiotic to kill bacteria using the reactive oxygen species (ROS) generated by Fenton-like reaction. However, its activity is still unsatisfied and requires large amount of hydrogen peroxide with side effects toward normal tissues. Herein, spherical mesoporous Fe-N-C single-atom nanozyme (SAzyme) is designed for antibacterial therapy via photothermal treatment enhanced Fenton-like catalysis process. Due to the large pore size (4.0 nm), high specific surface area (413.9 $m^2\ g^{-1}$) and uniform diameter (100 nm), the catalytic performance of Fe-N-C SAzyme is greatly improved. The Michaelis-Menten constant (K_m) is 4.84 mmol L^{-1}, which is similar with that of horseradish peroxidase (3.7 mmol L^{-1}). Moreover, mesoporous Fe-N-C SAzyme shows high photothermal conversion efficiency (23.3 %) owing to the carbon framework. The catalytic activity can be enhanced under light irradiation due to the elevated reaction temperature. The bacteria can also be killed via physical heat effect. Due to the synergistic effect of nanozyme catalysis and photothermal treatment, the antibacterial performance is much higher than that using single antibacterial method. This work provides an alternative for combined antibacterial treatment via photothermal treatment assisted catalytic process using spherical mesoporous single-atom nanozyme as an antibiotic.

* Corresponding authors.
E-mail addresses: qinyue@uestc.edu.cn (Q. Yue), jingwei@xjtu.edu.cn (J. Wei).

https://doi.org/10.1016/j.jcis.2021.08.054
0021-9797/

1. Introduction

The disease and safety of medical equipment caused by bacterial infection are threatening human health all over the world.[1] Antibiotics have been widely used in the therapy of bacterial infections. However, antibiotics have certain cytotoxicity and side effects.[2–4] There are many safety concerns associated with the excessive use of antibiotics. Most importantly, the misuse of antibiotics can lead to the development of antimicrobial resistance.[5] Hydrogen peroxide can be converted to hydroxyl radicals via Fenton-like reaction. As a kind of reactive oxygen species (ROS), hydroxyl radicals can effectively cause oxidative damage to the cell membrane and cell wall of bacteria to achieve effective antibacterial application.[6] However, there are still many problems for antibacterial treatment via Fenton-like reaction. For example, Fenton-like reaction needs to introduce high dose of hydrogen peroxide. High level of hydrogen peroxide will damage the normal tissue and hinder the wound healing.[7,8] If the physiological concentration of hydrogen peroxide is used, the amount of ROS produced will be too less to kill bacteria effectively.

Nanozymes have been recognized as a promising antibacterial agent in recent years.[9] They can act as a catalyst to generate ROS to achieve broad-spectrum antibacterial therapy. Different from Fenton reaction, the catalytic generation of ROS is mainly based on various enzyme catalytic activities of nanozymes themselves, such as oxidase-like (OXD) and peroxidase-like (POD) activities. They usually use oxygen or hydrogen peroxide as a catalytic substrate, achieving the production of ROS for antibacterial treatment.[9,10] Since nanozymes are usually metals,[11–15] metal oxides,[16–22] metal sulfides,[23–29] carbon-based materials [30–32] and metal–organic frameworks.[33–35] Nanozymes have many advantages that natural enzymes do not possess. Compared with horseradish peroxidase (HRP), POD-like nanozymes could still catalyze H_2O_2 after the treatment of extreme pH and temperature conditions, while HRP did not show any catalysis activity.[36] Nanozyme also has other advantages, such as high stability, low price and easy storage. They can still exert catalytic performance under extreme pH and temperature conditions.[37–39] Single-atom nanozyme (SAzyme), as a kind of nanozyme with ultrahigh catalytic performance, is based on the structure of natural enzyme in the form of single atom. With metal atoms as the active sites, SAzyme can effectively improve the atom utilization rate and increase the density of active sites.[40–45] Recently, SAzyme has been extensively studied for antibacterial treatment. For example, Xu *et al.*[42] used zinc-based zeolitic-imidazolate-framework (ZIF-8) as a precursor to synthesize carbon nanoparticles with a Zn-centered porphyrin-like structure, which exhibited peroxidase-like activity. They had higher catalytic performance than those of pure Fe_3O_4 and nanocarbon materials due to the presence of single Zn atom active sites within the materials. Huang *et al.*[45] prepared a single-atom nanozyme simulated the axial ligand-coordination structure of N atoms in natural heme. It has carbon framework and confined axial *N*-coordinated single-atom Fe. The oxidase-like catalytic activity was 70 times higher than that of commercial Pt/C with normalized metal content. It was successfully used for antibacterial therapy in mouse skin wound models. Despite great progresses, it still suffers some problems. The catalytic performance of SAzyme is inferior to that of natural enzymes. SAzyme has lower metal atom content, especially for reported SAzyme, which may be one reason for the limitation of the catalytic performance. Moreover, most of SAzyme materials were prepared using metal–organic framework as a precursor. The microporous framework is not beneficial for the fast mass transport due to the small pore size.

Spherical mesoporous materials with large pore size (2–50 nm), uniform spherical morphology, and low transfer resistance have attracted broad interests.[46] The mesoporous framework can significantly increase the specific surface area, promote the mass transport and expose abundant active sites for catalyst. It's anticipated that spherical mesoporous SAzyme materials would inherit the advantages of both spherical mesoporous materials and SAzyme, which would exhibit fascinating properties in biosensor and biomedicine.[47] Generally, such spherical mesoporous SAzyme materials show four advantages. Firstly, spherical mesoporous SAzyme shows large specific surface area.[48] The metal sites can be fully exposed and utilized. Therefore, the peroxidase-like activity can be improved. More numbers of ROS can be generated, which can effectively kill bacteria. Secondly, spherical mesoporous SAzyme showed uniform diameter and large pore size,[46] which favor the mass transport inside the materials.[49] The reactants can easily contact with the active sites. The catalytic performance can be enhanced. Thirdly, spherical mesoporous SAzyme with carbon framework also exhibit excellent photothermal properties due to the light absorbance ability of carbon materials.[50] Under near-infrared light irradiation, the temperature of spherical mesoporous SAzyme can be increased, which can enhance the catalytic activity.[51–53] High temperature can also bring antibacterial activity in a physical manner.[54,55] Fourthly, spherical mesoporous SAzyme can act as a nanocontainer or nanoreactor.[56] Due to the large mesoporous size, some large guest molecules (*e.g.*, enzyme) or nanoparticles (*e.g.*, Au nanoparticles, quantum dots) can be encapsulated in the mesopores.[57] These hybrid materials would exhibit enhanced performance and multifunction. Due to the above advantages, spherical mesoporous SAzyme would be an ideal candidate for antibacterial or other biomedical applications based on properties of nanozyme. However, there are very few studies on the synthesis and biomedical applications for spherical mesoporous nanozyme, especially SAzyme.

Herein, spherical mesoporous Fe-N-C single-atom nanozyme with large pore size (4.0 nm), high specific surface area (413.9 $m^2\ g^{-1}$) and uniform diameter (100 nm) is synthesized via a soft-template strategy for antibacterial application (Scheme 1). Spherical mesoporous SAzyme exhibits high peroxidase-like catalytic activity with Michaelis-Menten constant (K_m) of 4.84 mmol L^{-1} toward H_2O_2 and photothermal performance with photothermal conversion efficiency of 23.3 %. The temperature of the SAzyme catalyst is increased under light irradiation. It further improves the peroxidase-like catalytic activity with the increase of temperature. Simultaneously, the produced ROS converted from hydrogen peroxide can destroy the cell membrane and improve the sensitivity and permeability of bacteria to heat. Therefore, spherical mesoporous Fe-N-C SAzyme exhibits high antibacterial ability via photothermal treatment and catalytic antibacterial. Finally, *in vivo* antibacterial experiments on mouse skin wounds show that the spherical mesoporous SAzyme can avoid bacterial infections and increase the healing rate of wounds.

2. Materials and methods

2.1. Materials

Dopamine hydrochloride (≥99.0 %), $(NH_4)_2Fe(SO_4)_2{\cdot}6H_2O$ (≥99.5 %) and 1,3,5-trimethylbenzene (≥99.0 %) were purchased from Shanghai TITAN Technology Co., Ltd. 3,3′,5,5′-tetramethylbenzidine (TMB, 99.0 %), terephthalic acid (TA, 99 %) and tryptone (BioReagent) were purchased from Macklin Biochemical Co., Ltd. Ethanol (≥99.5 %) and ammonia solution (25–28 %) were purchased from Tianjin Zhiyuan Chemical Co., Ltd. Pluronic F127

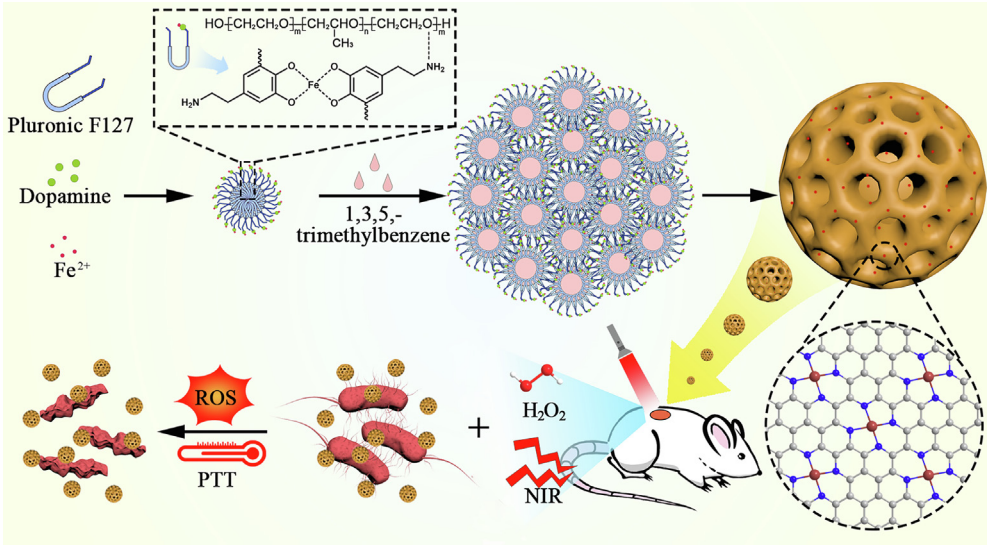

Scheme 1. Schematic illustration of the synthesis and antibacterial application for spherical mesoporous Fe-N-C single-atom nanozyme.

(BioReagent) was purchased from Sigma-Aldrich Shanghai Trading Co., Ltd. Glycerol (99.5 %) and sodium chloride (≥99.5 %) were purchased from Shanghai Aladdin reagent Co., Ltd. Agar powder (BioReagent) was purchased from Solarbio Science & Technology Co., Ltd. Yeast extract and SYTO9 green fluorescent nucleic acid stain (5 mM in DMSO) were purchased from Thermo Fisher Scientific Co., Ltd. Potassium dihydrogen phosphate (KH_2PO_4, ≥ 99.5 %), dipotassium hydrogen phosphate (K_2HPO_4, ≥ 99 %) and paraformaldehyde (≥95.0%) were purchased from Sinopharm Chemical Reagent Co., Ltd. Acetate buffer solution (pH = 4) was purchased from Guangzhou Zhencui Quality Inspection Technology Service Co., Ltd. Propidium iodide (PI, 1 mg/mL) was purchased from Shanghai Ruichu Biotechnology Co., Ltd. Chloral hydrate solution (10 %) was purchased from Fuzhou Brunei Biotechnology Co., Ltd. All reagents were used without further purification.

2.2. Synthesis of spherical mesoporous Fe-N-C SAzyme

Pluronic F127 (1.0 g) and dopamine hydrochloride (0.5 g) were dissolved into the mixture of ethanol (50 mL) and water (50 mL) under ultrasonication. Then, $(NH_4)_2Fe(SO_4)_2{\cdot}6H_2O$ (3.92 g) and 1,3,5-trimethylbenzene (2.0 mL) were added. After 30 min, $NH_3{\cdot}H_2O$ (5.0 mL, 28 %) was added drop by drop. After stirring for 30 min, the mixture was centrifuged and washed for three times. The collected products were dried in vacuum oven at 60 °C to obtain the composited powder. The products were calcinated in nitrogen atmosphere at 350 °C for 3 h, and then at 800 °C for another 5 h with the heating rate of 1 °C min^{-1}. Finally, spherical mesoporous Fe-N-C SAzyme was obtained.

2.3. Characterizations

Scanning electron microscopy (SEM) images were recorded on a Gemini SEM 500 and Gemini SEM 300. Transmission electron microscopy (TEM) results were taken using a JEM-F200 at 200 kV. X-ray photoelectron spectroscopy (XPS) results were detected by a Kratos AXIS Ultra DLD system with Al K_α radiation as an X-ray source. X-ray diffraction (XRD) patterns were collected on a Bruker D8 Advance with Cu K_α (λ = 1.54 Å) in the 2θ range of 10-80 ° and the scanning speed was 10 ° min^{-1}. Raman spectra were conducted on a Horiba Scientific LabRAM Raman NSOM with the 633 nm wavelength excitation at the range of 800–2000 cm^{-1}. The Brunauer-Emmett-Teller (BET) method was used to calculate the specific surface area, tested by Micromeritics Tristar 3020 at −196 °C.

2.4. Peroxidase-like catalysis and photothermal performance

TA was used to detected ·OH. The total volume of the reaction system was 1.0 mL. The concentrations of spherical mesoporous Fe-N-C SAzyme, hydrogen peroxide and TA were 100 μg mL^{-1}, 10 mmol L^{-1} and 0.5 mmol L^{-1}, respectively. The pH value of the buffer was 4. The reaction was carried out at room temperature. After incubation for 2 h, the fluorescence spectra in different systems was detected. The excitation wavelength of the TA was 315 nm. The emission wavelength was around 435 nm.

The total volume of the reaction system was 1.0 mL. The concentrations of spherical mesoporous Fe-N-C SAzyme, hydrogen peroxide and TMB were 20 μg mL^{-1}, 10 mmol L^{-1} and 0.8 mmol L^{-1}, respectively. The pH value of the buffer was 4. The reaction was carried out at room temperature. Then the peroxidase-like activities of Fe-N-C SAzyme with different concentrations, pH buffer systems and temperature were tested. The Michaelis-Menten constant (K_m) of the Fe-N-C SAzyme was determined. The catalysis system was tested with different concentrations of H_2O_2. The kinetic curves were measured at 652 nm in 10 min. The specific calculation method was as following equation (Equation (1)):

$$v_0 = \frac{\Delta A}{kb\Delta t} \quad (1)$$

where v_0 was initial velocities. k was molar extinction coefficient of oxTMB. b was optical length. In this case, k value of oxTMB was 39000 M^{-1} cm^{-1}.[58] b was 1 cm. Δt was 5 s and ΔA was the change of absorbance in the first 5 s. Then, the initial velocities-absorbance curves can be fitted with Michaelis-Menten equation (Equation (2)) as following:

$$v_0 = \frac{V_{max} \cdot [S]}{K_m + [S]} \quad (2)$$

Finally, the Michaelis-Menten Constant (K_m) of mesoporous Fe-N-C SAzyme with hydrogen peroxide as substrate was calculated to be 4.84 mmol L^{-1}. V_{max} was 0.118 μmol L^{-1} s^{-1}.

K_{cat} was calculated by the following equation (Equation (3)):

$$K_{cat} = \frac{V_{max}}{[E]} \quad (3)$$

where [E] was the molar concentration of Fe atom, which was 10.744 μmol L^{-1}. Finally K_{cat} was calculated as 0.0110 s^{-1}.

Photothermal properties of spherical mesoporous Fe-N-C SAzyme was evaluated. The total volume of the reaction system was 1.0 mL. The concentration of Fe-N-C SAzyme was 100 μg mL^{-1}. The power density of 808 nm near infrared laser was 1.5 W cm^{-2}. The heating time was 10 min. The photothermal properties of Fe-N-C SAzyme were tested with different concentrations and power densities. The stability of the material was also tested. The cooling curve of the material was measured. The photothermal conversion efficiency (η) of the mesoporous Fe-N-C SAzyme was calculated. [59] The η value was calculated by the following equation (Equation (4)):

$$\eta = \frac{hA(\Delta T_{max} - \Delta T_{max,H_2O})}{I(1 - 10^{-A_\lambda})} \quad (4)$$

where h was the heat transfer coefficient. A was the surface area of the container. ΔT_{max} was the temperature change of mesoporous Fe-N-C SAzyme solution at maximum steady-state temperature. $\Delta T_{max,H_2O}$ was the temperature change of water under the same condition at maximum steady-state temperature. I was laser power density. A_λ was the absorbance of mesoporous Fe-N-C SAzyme at 808 nm.

In the above equation, only hA was unknown. θ was defined as $\frac{\Delta T}{\Delta T_{max}}$. hA can be calculated by the following equation (Equation (5)):

$$t = -\frac{\sum_i m_i C_{p,i}}{hA} ln\theta \quad (5)$$

where t was the cooling time. m_i was the mass of water and mesoporous Fe-N-C SAzyme. $C_{p,i}$ was the heat capacity of the water and mesoporous Fe-N-C SAzyme. Because the mass of mesoporous Fe-N-C SAzyme is much lower than that of water, the equation can be simplified as (Equation (6)):

$$t = -\frac{m_{H_2O} C_{H_2O}}{hA} ln\theta \quad (6)$$

then, according to the cooling curve, hA can be calculated.

In this case, ΔT_{max} was 29.6 °C. $\Delta T_{max,H_2O}$ was 9.8 °C. I was 1.5 W cm^{-2}. A_λ was 0.498. m_{H_2O} was 1.0 × 10^{-3} kg. C_{H_2O} was 4.2 × 10^3 J kg^{-1} $°C^{-1}$. hA was 0.01207. Therefore, the η of mesoporous Fe-N-C SAzyme was calculated as 23.3 %.

2.5. Antibacterial performance in vitro

E. coli and *S. aureus* were used as representative of Gram-negative and Gram-positive bacteria, respectively. The bacteria were cultured at 37 °C overnight. The concentration of bacteria was 10^8 CFU mL^{-1} according to OD_{600} value. The whole experiment was divided into seven groups (n = 3): group I: blank; group II: Fe-N-C SAzyme; group III: H_2O_2; group IV: 808 nm NIR; group V: Fe-N-C SAzyme + H_2O_2; group VI: Fe-N-C SAzyme + 808 nm NIR; group VII: Fe-N-C SAzyme + H_2O_2 + 808 nm NIR. The antibacterial tests were carried out in 24 well plate. The total volume of the solution was 1.0 mL. The concentrations of bacterial suspension, Fe-N-C SAzyme and hydrogen peroxide were 10^7 CFU mL^{-1}, 100 μg mL^{-1} and 200 μmol L^{-1}, respectively. The pH value of buffer was 6. The power density was 1.5 W cm^{-2}. The irradiation time was 10 min. After 4 h, the remaining bacterial suspension was diluted and inoculated on the agar LB plates prepared in advance. The culture was continued overnight at 37 °C. The number of colonies was counted.

After the same methods used to treat bacteria with spherical mesoporous Fe-N-C SAzyme, the bacteria were collected by centrifugation and stained with 5 μmol L^{-1} of PI and 3 μmol L^{-1} of SYTO9 for 15 min, respectively. The bacteria were washed for several times and dispersed in glycerin for fluorescence imaging. The excitation wavelength of PI was 535 nm. The emission wavelength was 615 nm. The excitation wavelength of SYTO9 was 488 nm while the emission wavelength was 525 nm.

2.6. Antibacterial performance in vivo

The Kunming mice (KM mice, ~20 g, male) were purchased from the Experimental Animal Center of Xi'an Jiaotong University. All procedures were followed the guidelines of The Care and Use of Laboratory Animals of the Medical Research Council of Xi'an Jiaotong University. The mice were randomly divided into 7 groups (n = 3): group I: blank; group II: Fe-N-C SAzyme; group III: H_2O_2; group IV: 808 nm NIR; group V: Fe-N-C SAzyme + H_2O_2; group VI: Fe-N-C SAzyme + 808 nm NIR; group VII: Fe-N-C SAzyme + H_2O_2 + 808 nm NIR. The wounds with a diameter of about 5 mm were cut on the skin of mice by using a perforator. Then 100 μL of *S. aureus* suspension (10^8 CFU mL^{-1}) was added to the wound. After 24 h, the bacteria-infected wounds were treated with different treatments. The wound area was recorded every day. On the fifth day, the mice were sacrificed and the skin tissue of the wound was taken for histopathological H&E staining analysis.

2.7. Toxicity of spherical mesoporous Fe-N-C SAzyme

The KM mice were intravenously injected with Fe-N-C suspension (5 mg kg^{-1}). On the fifth day after the injection, the mice were sacrificed. The whole blood was obtained by heart blood collection. The serum was obtained by centrifugation for hematology analysis. The main organs of mice were removed and fixed with 4 % paraformaldehyde for subsequent use in histological analysis.

3. Results and discussion

3.1. Characterization of spherical mesoporous Fe-N-C SAzyme

Spherical mesoporous Fe-N-C SAzyme was synthesized via soft-template strategy. In alkaline ethanol/water solution, dopamine was used as carbon and nitrogen source. Pluronic F127 was used as a soft template. 1,3,5-trimethylbenzene was used as a pore swelling agent. Due to the strong hydrogen bonding between dopamine and polyethylene oxide (PEO) segments of F127, dopamine molecules were deposited on the surface of F127 micelles. To anchor the iron singe atom, iron species (Fe^{2+}) were used as an iron source to coordinate with catechol groups from dopamine. Due to the self-polymerization property of dopamine in the alkaline conditions in the presence of oxygen, the block polymer micelles/iron-polydopamine composited spheres were obtained. During the subsequent carbonization process, the block copolymers were decomposed, leaving plenty of mesopores. Iron-polydopamine networks were converted into nitrogen-doped carbon framework. The iron species were coordinated with nitrogen atoms to form Fe-N-C composites.

Scanning electron microscope (SEM) images of spherical mesoporous Fe-N-C SAzyme showed regular spherical morphology with diameter of around 100 nm (Fig. 1**a and 1b**). The large mesopores were distinctly distributed on the surface of the spheres. Transmission electron microscope (TEM) image (Fig. 1**c and 1d**) further confirmed the formation of spherical mesoporous structure. TEM results showed that no large iron nanoparticles were imbedded in the amorphous carbon framework. Fe element was more likely existed in the form of Fe atoms. The existence of iron atoms in the carbon material was proved by aberration-corrected atomic resolution high-angle annular dark-field scanning transmission electron microscopy (Fig. 1**e**). According to the element mapping

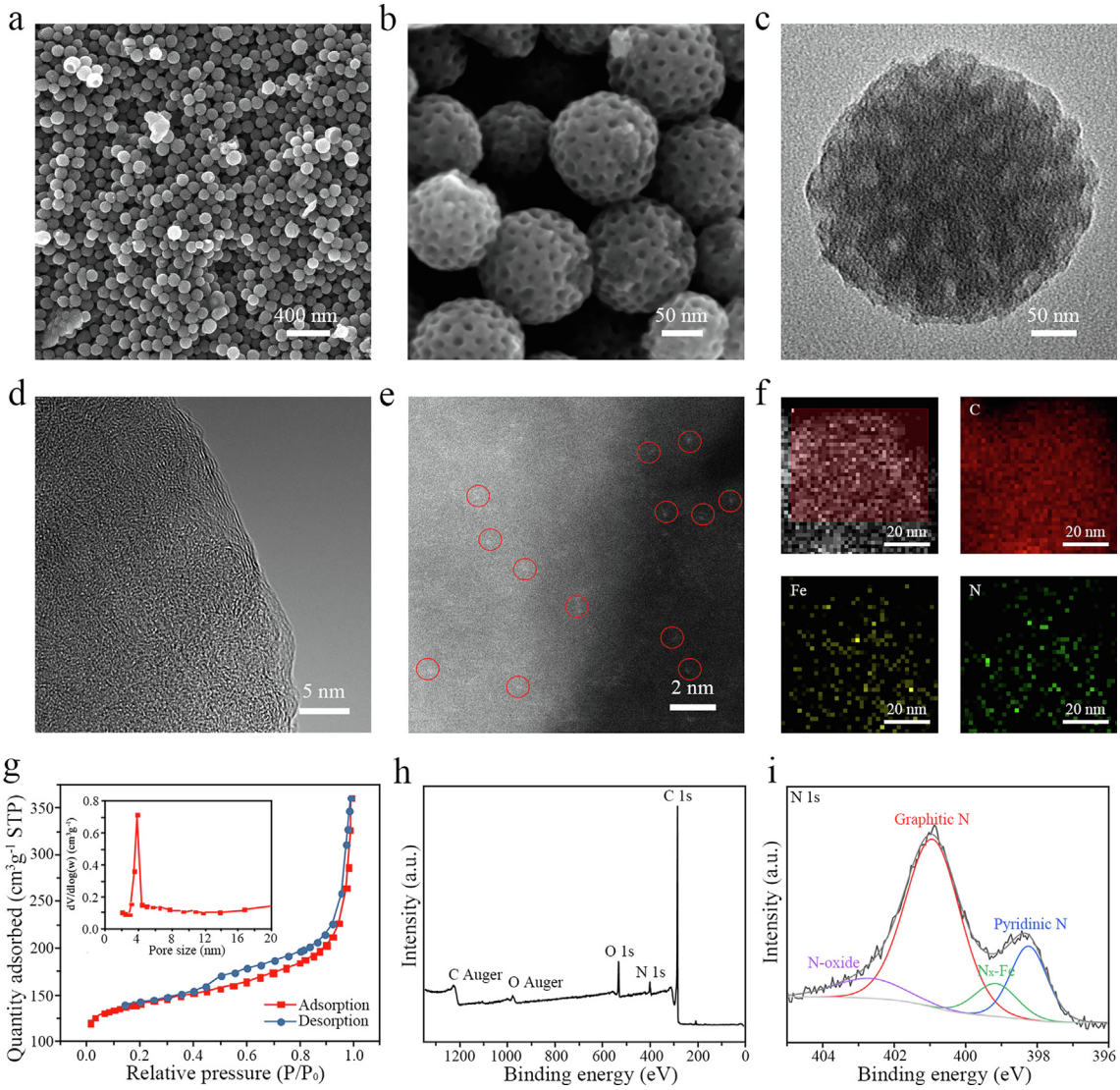

Fig. 1. Characterization of spherical mesoporous Fe-N-C SAzyme. (a, b) SEM images, (c) TEM image, (d) HRTEM image, (e) STEM image, (f) elemental mapping, (g) N_2 sorption isotherms and pore size distributions, (h) XPS spectra and (i) N 1 s spectra for spherical mesoporous Fe-N-C SAzyme.

analysis, Fe, N and C elements were distributed in the materials uniformly (Fig. 1**f**).

Nitrogen adsorption–desorption isotherms of SAzyme revealed a typical mesoporous framework. The pore size and specific surface area were 4.0 nm and 413.9 $m^2\ g^{-1}$, respectively (Fig. 1**g**). X-ray diffraction (XRD) patterns of spherical mesoporous Fe-N-C SAzyme showed two broad peaks, which were ascribed to 002 and 101 planes of carbon (**Figure S1**). There was no peak for iron/iron oxide/iron carbide crystal, indicating that the iron species were distributed in the mesoporous carbon framework uniformly without any aggregation or crystallization. Raman spectra for spherical mesoporous Fe-N-C SAzyme showed G and D band at around 1591 and 1351 cm^{-1}, respectively (**Figure S2**), indicating a carbon framework. X-ray photoelectron spectroscopy (XPS) analysis of spherical mesoporous Fe-N-C SAzyme showed the presence of C, O and N (Fig. 1**h**). C 1 s spectra can be divided into three peaks, which were ascribed to C═C, C—C and C—N bond, respectively (**Figure S3a**).[45] N 1 s spectra can be divided into four peaks, which were ascribed to pyridinic N (18.4 %), N_x-Fe bond (9.6 %), graphitic N (62.6 %) and N oxides (9.42 %), respectively (Fig. 1**i**).[60] Fe 2p spectra revealed two weak peaks of Fe $2p_{1/2}$ and Fe $2p_{3/2}$ (**Figure S3b**).

3.2. Enzyme-like activity of spherical mesoporous Fe-N-C SAzyme

Peroxidase-like activity for spherical mesoporous Fe-N-C SAzyme was evaluated. Firstly, the fluorescence probe of terephthalic acid (TA) was used to verify that ROS was hydroxyl radical (·OH) (**Figure S4**). In this process, hydrogen peroxide was converted to ·OH with the assistance of SAzyme. 3,3′,5,5′-tetramethyl benzidine (TMB) was used as a chromogenic substrate to detect ·OH. TMB can be oxidized by ·OH and turn into oxTMB with blue color in solution. The absorbance value was positively correlated with the concentration of ·OH in the system. The absorbance of the solution at 652 nm was changed when the concentration of SAzyme was changed (Fig. 2**a**). When the concentration of Fe-N-C SAzyme increased, the numbers of ·OH generated by catalysis gradually increased. The corresponding photographs also confirmed the color change of the reaction system (Fig. 2**a, inset**). The catalytic activity of spherical mesoporous Fe-N-C SAzyme materials under different pH values was also investigated. The spherical mesoporous Fe-N-C SAzyme showed the best catalytic performance at pH value of 4. In the near neutral conditions, mesoporous Fe-N-C SAzyme has little peroxidase-like activity (Fig. 2**b**). The Michaelis-Menten constant (K_m) of spherical mesoporous

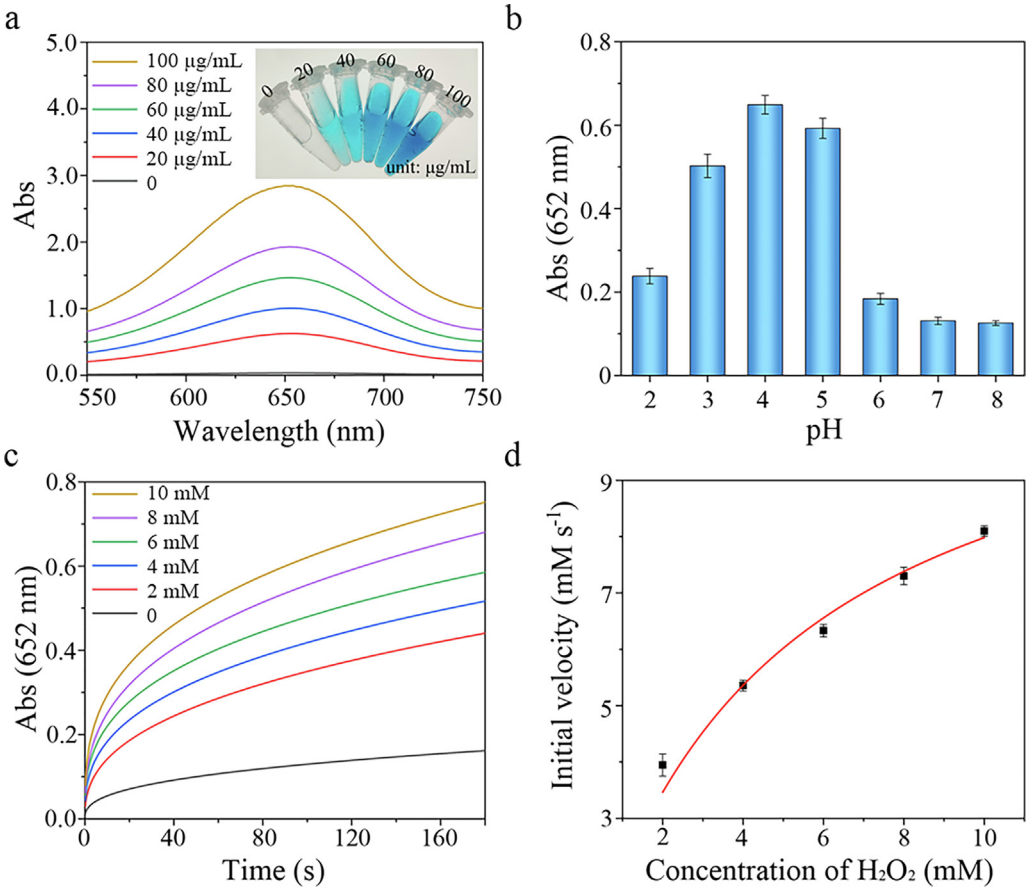

Fig. 2. Enzyme-like activity of spherical mesoporous Fe-N-C SAzyme. (a) UV–vis spectra for TMB chromogenic curves with different concentrations of Fe-N-C SAzyme. Inset in (a) was the corresponding photograph of reaction system. (b) The absorbance at 652 nm for TMB chromogenic reaction system at different pH conditions. (c) UV–vis spectra for TMB chromogenic kinetics curves of different concentration of H_2O_2 catalyzed by Fe-N-C SAzyme. (d) Steady-state kinetic assay of Fe-N-C SAzyme with H_2O_2 as substrate. Experimental conditions: 0.8 mmol L^{-1} TMB, 10 mmol L^{-1} H_2O_2, 20 μg mL^{-1} Fe-N-C.

Fe-N-C SAzyme was 4.84 mmol L^{-1} with H_2O_2 as a substrate (Fig. 2**c, d,** **Figure S5**), which was comparable to the K_m of horseradish peroxidase (3.7 mmol L^{-1}).[36] V_{max} and K_{cat} was calculated as 0.118 μmol L^{-1} s^{-1} and 0.0110 s^{-1}, respectively. The catalytic activity for spherical Fe-N-C SAzyme was among the best of other reported state-of-the-art single-atom nanozyme (**Table S1**). The pH value of the infected wound is slightly acidic due to bacterial metabolites.[61] The catalytic performance of spherical mesoporous Fe-N-C SAzyme exhibited weak catalytic performance like other nanozyme in bacterial microenvironment. Therefore, the antibacterial performance was usually limited. However, the catalytic performance was also related to the reaction temperature. The catalytic performance can be enhanced by increasing the reaction temperature. Luckily, the mesoporous carbon framework showed excellent photo adsorption ability. It's possible to increase the temperature via near-infrared light irradiation.

3.3. Photothermal performance of spherical mesoporous Fe-N-C SAzyme

To further increase the catalytic performance of spherical mesoporous SAzyme, the photothermal property of SAzyme was investigated. Fe-N-C SAzyme can absorb the photo energy due to its carbon framework (**Figure S6**). The absorbance was positively correlated with the concentration of Fe-N-C SAzyme. When near-infrared light (NIR) at 808 nm was used as a light source. The temperature of the solution increased gradually when the irradiation time increased. The final temperature of the solution was dependent on the concentration of Fe-N-C SAzyme (**Figure S7**). For example, the temperature increased to 55.3 °C when 100 μg mL^{-1} of Fe-N-C SAzyme solution was irradiated for 600 *s* under the power density of 1.5 W cm^{-2}. When the power density of NIR light increased from 0.5 to 2.0 W cm^{-2}, the final temperature of solution increased from 34.5 to 61.9 °C (Fig. 3**a**). The temperature change of the material in the photothermal process was clearly seen through the thermal imaging photos (Fig. 3**b**). The photothermal conversion efficiency (η) of Fe-N-C SAzyme was 23.3 % (Fig. 3**c**), which was comparable to other carbon-based nanomaterials, such as carbon dots, carbon nanotubes and graphene materials (**Table S2**). The Fe-N-C SAzyme also showed excellent photothermal stability (Fig. 3**d**). When the reaction temperature increased, the catalytic activity increased due to the enhanced reaction kinetics (Fig. 3**e**). Subsequently, the photothermal treatment assisted catalysis performance of Fe-N-C SAzyme was investigated. The localized heat around the spherical mesoporous Fe-N-C SAzyme effectively enhanced the POD-like activities and produced more numbers of ROS (Fig. 3**f**). The catalytic performance of spherical mesoporous Fe-N-C SAzyme with or without 808 nm NIR irradiation for 600 *s* was evaluated (Fig. 3**g**). The catalytic performance of spherical mesoporous Fe-N-C SAzyme with near-infrared irradiation was 2 times higher than that without light irradiation. This result revealed that light irradiation could enhance the catalytic performance. Therefore, it was possible to regulate the catalytic performance by light. Moreover, the photothermal treatment can also lead to the physical damage to the bacteria, which is also helpful to combat bacteria.

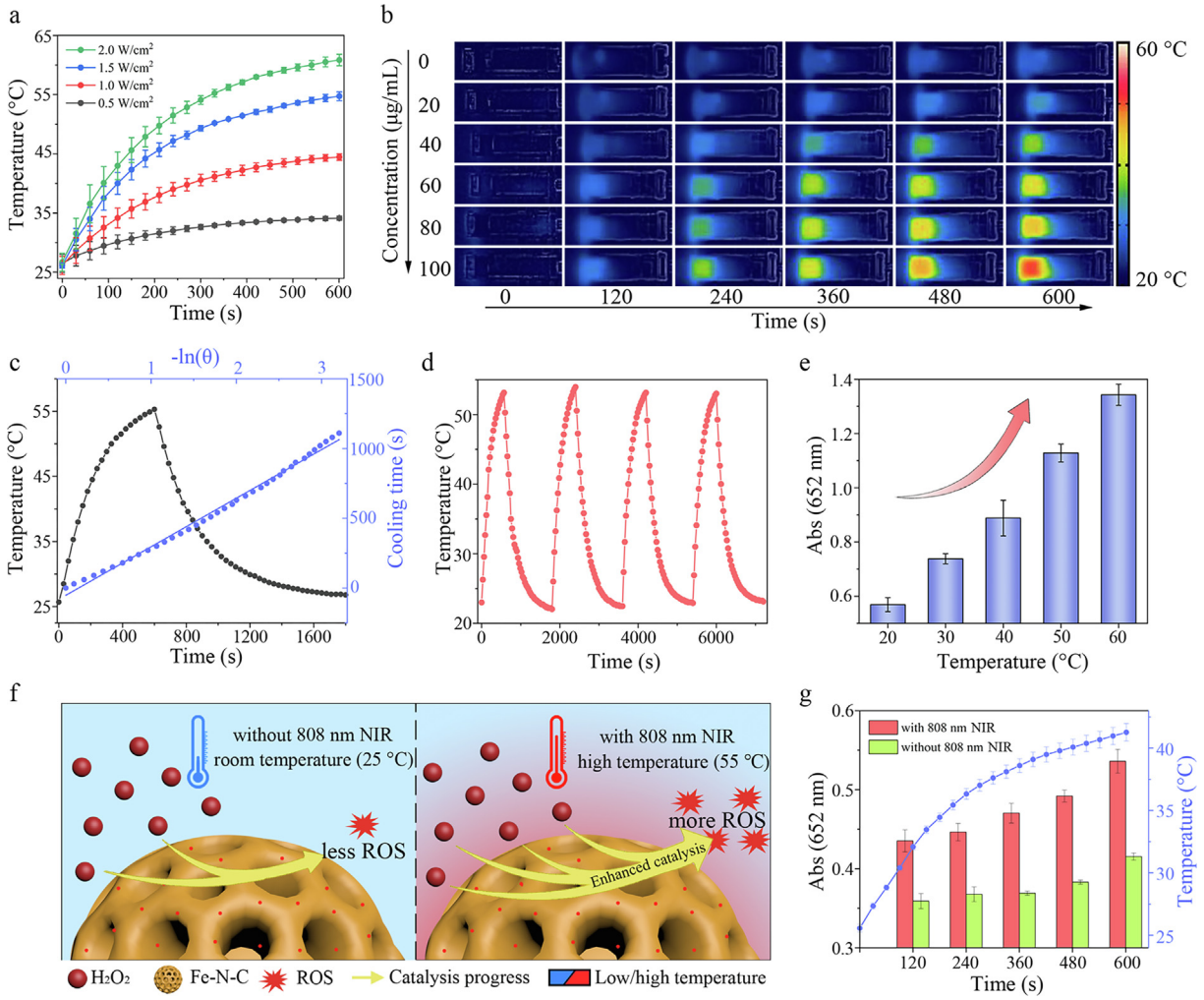

Fig. 3. Photothermal performance of spherical mesoporous Fe-N-C SAzyme. (a) Temperature change curves of Fe-N-C SAzyme solution under 808 nm irradiation with varied laser power densities. (b) Thermographic images of Fe-N-C SAzyme solution under 808 nm irradiation with varied Fe-N-C SAzyme concentrations at different time. Laser power density was 1.5 W cm^{-2}. (c) Photothermal conversion efficiency and cooling curve. (d) Temperature elevation curves over four cycles of 808 nm NIR laser on/off irradiation. (e) The absorbance at 652 nm of the solution at different temperature. (f) Schematic illustration of the synergistic effects of photothermal treatment and catalysis. (g) Photothermal temperature values and absorbance at 652 nm of Fe-N-C SAzyme solution with and without 808 nm irradiation. If not mentioned, the time of 808 nm NIR treatment was 10 min. The concentration of Fe-N-C SAzyme was 100 μg mL^{-1}. The laser power density was 1.5 W cm^{-2}.

3.4. Antibacterial performance in vitro

Spherical mesoporous Fe-N-C SAzyme exhibited peroxidase-like catalytic and photothermal performance. Then *Escherichia coli* (*E. coli*) and *Staphylococcus aureus* (*S. aureus*) were used as the typical Gram-negative and Gram-positive bacteria to evaluate the antibacterial performance of spherical mesoporous Fe-N-C SAzyme with the assistance of H_2O_2. The antibacterial experiment was carried out at pH 6. To compare the different photothermal and catalytic antibacterial performance, the treatments were divided into seven groups: group I: blank; group II: Fe-N-C SAzyme; group III: H_2O_2; group IV: 808 nm NIR; group V: Fe-N-C SAzyme + H_2O_2; group VI: Fe-N-C SAzyme + 808 nm NIR; group VII: Fe-N-C SAzyme + H_2O_2 + 808 nm NIR. Among them, the concentration of Fe-N-C SAzyme solution and hydrogen peroxide were 20 μg mL^{-1} and 200 μmol L^{-1}, respectively. The irradiation time by 808 nm NIR was 10 min. The colonies were counted using spread plate method. Comparing with the blank group, group II-IV showed no antibacterial activity (Fig. 4**a**) and the bacteria activities were above 80 %. For group V, due to the peroxidase-like activity of Fe-N-C SAzyme, it could catalyze H_2O_2 to generate ·OH. Even at a very low concentration (200 μmol L^{-1}) of H_2O_2, it could produce enough ·OH to kill bacteria. However, due to the limitation of pH condition, the catalytic ability of Fe-N-C SAzyme cannot be fully activated. The bacteria activity only decreased to 64.3 % for *E. coli* and 57.5 % for *S. aureus*. The carbon framework can absorb near-infrared irradiation and convert it into heat energy, which can kill bacteria via heat effect. The bacteria activities of *E. coli* and *S. aureus* were 56.9 % and 56.8 % under light irradiation in group VI, respectively. The above results revealed that catalytic treatment and photothermal treatment alone cannot achieve high antibacterial effect. Therefore, the synergistic antibacterial performance via combined catalytic and photothermal treatment was further evaluated in group VII. The bacteria activities of *E. coli* and *S. aureus* decreased to 17.9 % and 11.9 %, respectively (Fig. 4**c**). Comparing with the catalytic and photothermal antibacterial method, bacteria could be effectively killed.

The morphologies of the bacteria before and after treatments were characterized by SEM (Fig. 4**b**). Comparing with other groups, most of *S. aureus* showed collapsed morphology in group VII. A large number of lysed bacteria was observed for *E. coli*. SYTO9 and propidium iodide (PI) were used to stain the live and dead bac-

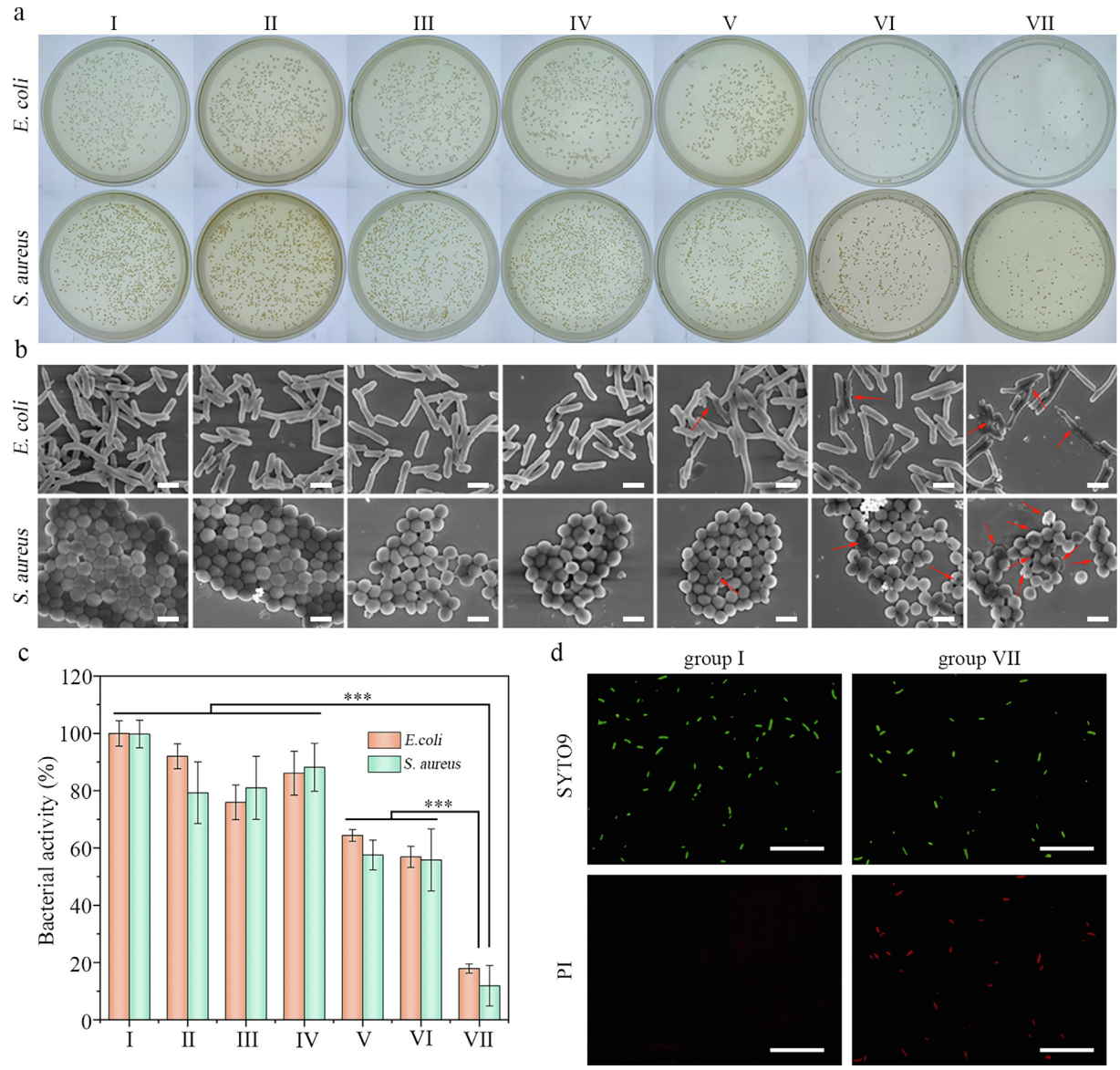

Fig. 4. Antibacterial performance *in vitro*. (a) Photographs of remaining *E. coli* and *S. aureus* colonies on agar plates in different groups (n = 3). (b) Corresponding SEM images of treated *E. coli* and *S. aureus*. Scale bar: 1 μm. (c) Corresponding bacterial activity after treatment in different groups (n = 3). (d) SYTO9/PI staining images of the above bacteria with and without treatments for 4 h. Scale bar: 20 μm. Group I: blank; group II: Fe-N-C SAzyme; group III: H_2O_2; group IV: 808 nm NIR; group V: Fe-N-C SAzyme + H_2O_2; group VI: Fe-N-C SAzyme + 808 nm NIR; group VII: Fe-N-C SAzyme + H_2O_2 + 808 nm NIR. Results are presented as mean ± S.D. (n = 3, $^{*}p < 0.05$, $^{**}p < 0.01$, $^{***}p < 0.001$, analyzed by Student's t-test).

teria, respectively (Fig. 4**d**). Most of *E. coli* remained alive in group I. By contrast, large numbers of *E. coli* in group VII showed red fluorescence, indicating that most of bacteria was dead.

3.5. Antibacterial performance in vivo

Encouraged by the excellent photothermal/catalytic synergistic antibacterial properties of the spherical mesoporous Fe-N-C SAzyme, the antibacterial performance *in vivo* was further investigated. Bacterial infection is one of the main reasons that hinder wound healing. The bacteria-infected wound mode was used. The wounds on the skin surface of mice were nicked and artificially infected with *S. aureus* (Fig. 5**a**). The mice were divided into 7 groups: group I: blank; group II: Fe-N-C SAzyme; group III: H_2O_2; group IV: 808 nm NIR; group V: Fe-N-C SAzyme + H_2O_2; group VI: Fe-N-C SAzyme + 808 nm NIR; group VII: Fe-N-C SAzyme + H_2O_2 + 808 nm NIR. After infected with *S. aureus* for 24 h, the wounds were treated for different days. The wound area of mice decreased gradually (Fig. 5**b**). In group I ~ IV, the wound area remained 30 % at the fourth day. For group V and group VI, they showed faster healing rate than group I-IV. The wound area decreased to 21 % and 26 %, respectively, indicating both photothermal and catalytic treatment can accelerate the healing process. In group VII, the healing rate was the fastest all over the whole groups. The wound area only remained 9 % compared with the first day. The skin on the back of mice was almost completely cured in group VII, indicating the combined treatment can further enhance the wound healing rate (Fig. 5**c**). The photothermal images and cooresponding temperature changing curve of bacterial treated sites proved that the localized temperature increased obviously after NIR irradiation (**Figure S8a, b**). There was almost no inflammatory cell infiltration from hematoxylin-eosin (H&E) staining in group VII compared to

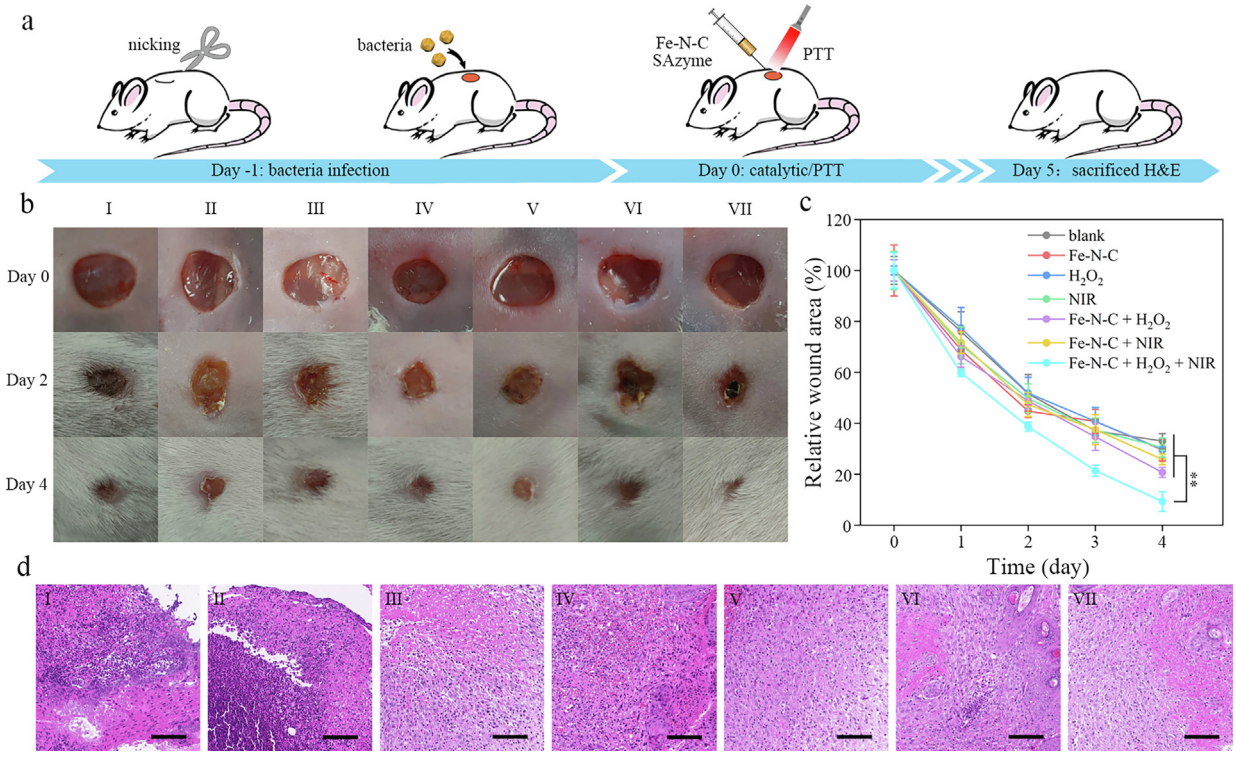

Fig. 5. Antibacterial performance *in vivo*. (a) Schematic illustration of wound healing experiment. (b) Photographs of *S. aureus* infected mice in different groups (n = 3) during the therapy progress. (c) Corresponding relative wound area. (d) Skin wound histopathological analysis on day 5. Scale bar: 100 μm. Group I: blank; group II: Fe-N-C SAzyme; group III: H_2O_2; group IV: 808 nm NIR; group V: Fe-N-C SAzyme + H_2O_2; group VI: Fe-N-C SAzyme + 808 nm NIR; group VII: Fe-N-C SAzyme + H_2O_2 + 808 nm NIR. Results are presented as mean ± S.D. (n = 3, $^*p < 0.05$, $^{**}p < 0.01$, $^{***}p < 0.001$, analyzed by Student's t-test).

the other groups and the epidermis cured completely (Fig. 5**d**). Spherical mesoporous Fe-N-C SAzyme has the excellent antibacterial performance.

3.6. Toxicity of spherical mesoporous Fe-N-C SAzyme

The toxicity of spherical mesoporous Fe-N-C SAzyme was investigated *in vivo*. 200 μL of Fe-N-C SAzyme (5 mg kg^{-1}) was injected into mice via tail vein for 5 days to observe the physiological state of mice. During this period, the weight of mice increased gradually. The growth rate of the mice weight in the control group and the experimental group was similar (**Figure S9**). The hematology analysis results revealed that all the blood parameters were in the normal range (**Figure S10**). On the fifth day, the mice were sacrificed and their main organs were sectioned for H&E staining to observe whether there were pathological changes. H&E staining showed that Fe-N-C SAzyme had no side effect on the main organs of mice (**Figure S11**). The above results revealed that Fe-N-C SAzyme showed negligible toxicity.

4. Conclusion

Spherical mesoporous Fe-N-C single-atom nanozyme with excellent peroxidase-like activity and photothermal property is developed via a soft-template strategy for antibacterial application. It is well known that mesoporous structure can greatly improve the properties of nanomaterials. [46,48,49] However, there are few reports on single-atom nanozymes with mesoporous structure. Therefore, we designed a kind of spherical Fe-single-atom nanozyme with mesoporous structure to achieve high catalytic activity. Compared with the reported single-atom nanozymes, [40–45,47] the obtained Fe-N-C SAzyme shows large pore size, high specific surface area and highly dispersed iron atoms, which facilitates the mass transport and exposure of active sites. Therefore, Fe-N-C SAzyme exhibits excellent peroxidase-like activity, which can covert H_2O_2 to highly toxic hydroxyl radicals. The peroxidase activity of the obtained material was close to that of natural HRP [36]. Moreover, the carbon framework shows excellent NIR absorbance and high photothermal conversion efficacy. Photothermal treatment can not only improve the catalytic activity of Fe-N-C SAzyme via the increasement of reaction temperature, but also be used to directly kill bacteria via a physical manner. The synergistic antibacterial effect of catalysis and photothermal treatment using spherical mesoporous Fe-N-C SAzyme can effectively kill the bacteria on the infected wound and accelerate the wound healing. This work provides a rational design of antibacterial materials using spherical mesoporous SAzyme with high photothermal and peroxidase-like catalysis performance. Due to the tunable compositions and mesoporous framework, such kind of spherical mesoporous SAzyme would be further functionalized and exhibit promosing applications in catalysis and biomedical fields.

CRediT authorship contribution statement

Youyou Feng: Investigation, Formal analysis, Writing – original draft, Writing – review & editing. **Jing Qin:** Investigation, Data curation, Writing – original draft. **Yu Zhou:** Investigation, Data curation. **Qin Yue:** Resources, Supervision. **Jing Wei:** Resources, Supervision, Writing – review & editing, Funding acquisition.

Declaration of Competing Interest

The authors declare that they have no known competing financial interests or personal relationships that could have appeared to influence the work reported in this paper.

Acknowledgements

This work was financially supported by the National Natural Science Foundation of China (No. 21701130), Key Research and Development Program of Shaanxi (Program No. 2021GY-225). We thank Mr. Zijun Ren at Instrument Analysis Center of Xi'an Jiaotong University for their assistance with SEM analysis.

Appendix A. Supplementary material

Supplementary data to this article can be found online at https://doi.org/10.1016/j.jcis.2021.08.054.

References

[1] H. Koo, R.N. Allan, R.P. Howlin, P. Stoodley, L. Hall-Stoodley, Targeting microbial biofilms: current and prospective therapeutic strategies, Nat. Rev. Microbiol. 15 (2017) 740.
[2] A.B. Coffin, E.W. Rubel, D.W. Raible, Bax, Bcl2, and p53 differentially regulate neomycin- and gentamicin-induced hair cell death in the zebrafish lateral line, J. Assoc. Res. Oto. 14 (2013) 645.
[3] Y.J. Park, J. Chang, G. Lee, J.S. Son, S.M. Park, Association of class number, cumulative exposure, and earlier initiation of antibiotics during the first two-years of life with subsequent childhood obesity, Metabolism 112 (2020) 154348.
[4] M. Angoa-Perez, D.M. Kuhn, Evidence for modulation of substance use disorders by the gut microbiome: Hidden in plain sight, Pharmacol. Rev. 73 (2021) 571.
[5] C. Willyard, Drug-resistant bacteria ranked, Nature 543 (2017) 15.
[6] Y. Hou, X.Y. Li, Q.D. Zhao, G.H. Chen, C.L. Raston, Role of hydroxyl radicals and mechanism of Escherichia coli inactivation on Ag/AgBr/TiO_2 nanotube array electrode under visible light irradiation, Environ. Sci. Technol. 46 (2012) 4042.
[7] F. Vatansever, W.C.M.A. de Melo, P. Avci, D. Vecchio, M. Sadasivam, A. Gupta, R. Chandran, M. Karimi, N.A. Parizotto, R. Yin, G.P. Tegos, M.R. Hamblin, Antimicrobial strategies centered around reactive oxygen species–bactericidal antibiotics, photodynamic therapy, and beyond, FEMS Microbiol. Rev. 37 (2013) 955.
[8] M.D. Labas, C.S. Zalazar, R.J. Brandi, A.E. Cassano, Reaction kinetics of bacteria disinfection employing hydrogen peroxide, Biochem. Eng. J. 38 (2008) 78.
[9] Y.Y. Li, W.X. Zhu, J.S. Li, H.T. Chu, Research progress in nanozyme-based composite materials for fighting against bacteria and biofilms, Colloid Surf. B 198 (2021) 111465.
[10] F. Gao, T.Y. Shao, Y.P. Yu, Y.J. Xiong, L. Yang, Surface-bound reactive oxygen species generating nanozymes for selective antibacterial action, Nat. Commun. 12 (2021) 745.
[11] S. Bhattacharyya, S.R. Ali, M. Venkateswarulu, P. Howlader, E. Zangrando, M. De, P.S. Mukherjee, Self-assembled Pd_{12} coordination cage as photoregulated oxidase-like nanozyme, J. Am. Chem. Soc. 142 (2020) 18981.
[12] J.Q. Xi, G. Wei, L.F. An, Z.B. Xu, Z.L. Xu, L. Fan, L.Z. Gao, Copper/carbon hybrid nanozyme: Tuning catalytic activity by the copper state for antibacterial therapy, Nano Lett. 19 (2019) 7645.
[13] Y.F. Liu, N. Nie, H.F. Tang, C.R. Zhang, K.Z. Chen, W. Wang, J.F. Liu, Effective antibacterial activity of degradable copper-doped phosphate-based glass nanozymes, ACS Appl. Mater. Interfaces 13 (2021) 11631.
[14] G. Fang, W.F. Li, X.M. Shen, J.M. Perez-Aguilar, Y. Chong, X.F. Gao, Z.F. Chai, C.Y. Chen, C.C. Ge, R.H. Zhou, Differential Pd-nanocrystal facets demonstrate distinct antibacterial activity against Gram-positive and Gram-negative bacteria, Nat. Commun. 9 (2018) 129.
[15] W.C. Hu, M.R. Younis, Y. Zhou, C. Wang, X.H. Xia, In situ fabrication of ultrasmall gold nanoparticles/2D MOFs hybrid as nanozyme for antibacterial therapy, Small 16 (2020) 2000553.
[16] Y. Wang, C. Chen, D. Zhang, J. Wang, Bifunctionalized novel Co-V MMO nanowires: Intrinsic oxidase and peroxidase like catalytic activities for antibacterial application, Appl. Catal. B-Environ. 261 (2020) 118256.
[17] Q.Z. Mu, Y.F. Sun, A.Y. Guo, X.Y. Xu, B.P. Qin, A.J. Cai, A bifunctionalized $NiCo_2O_4$-Au composite: Intrinsic peroxidase and oxidase catalytic activities for killing bacteria and disinfecting wound, J. Hazard. Mater. 402 (2021) 123939.
[18] Y. Huang, Y. Liu, S. Shah, D. Kim, A. Simon-Soro, T. Ito, M. Hajfathalian, Y. Li, J.C. Hsu, L.M. Nieves, F. Alawi, P.C. Naha, D.P. Cormode, H. Koo, Precision targeting of bacterial pathogen via bi-functional nanozyme activated by biofilm microenvironment, Biomaterials 268 (2021) 120581.
[19] K. Khulbe, K. Karmakar, S. Ghosh, K. Chandra, D. Chakravortty, G. Mugesh, Nanoceria-based phospholipase-mimetic cell membrane disruptive antibiofilm agents, ACS Appl. Bio Mater. 3 (2020) 4316.
[20] M.N. Karim, M. Singh, P. Weerathung, P. Bian, R. Zheng, C. Dekiwadia, T. Ahmed, S. Walia, E. Della Gaspera, S. Singh, R. Ramanathan, V. Bansal, Visible-light-triggered reactive-oxygen-species-mediated antibacterial activity of peroxidase-mimic CuO nanorods, *ACS Appl*, Nano Mater. 1 (2018) 1694.
[21] H.Y. Kim, K.S. Park, H.G. Park, Glucose oxidase-like activity of cerium oxide nanoparticles: Use for personal glucose meter-based label-free target DNA detection, Theranostics 10 (2020) 4507.
[22] S.R. Shi, S. Wu, Y.R. Shen, S. Zhang, Y.Q. Xiao, X. He, J.S. Gong, Y. Farnell, Y. Tang, Y.X. Huang, L.Z. Gao, Iron oxide nanozyme suppresses intracellular Salmonella Enteritidis growth and alleviates infection in vivo, Theranostics 8 (2018) 6149.
[23] F. Wei, X.Y. Cui, Z. Wang, C.C. Dong, J.D. Li, X.J. Han, Recoverable peroxidase-like Fe_3O_4@MoS_2-Ag nanozyme with enhanced antibacterial ability, Chem. Eng. J. 408 (2021) 127240.
[24] W.Y. Yin, J. Yu, F.T. Lv, L. Yan, L.R. Zheng, Z.J. Gu, Y.L. Zhao, Functionalized nano-MoS_2 with peroxidase catalytic and near-infrared photothermal activities for safe and synergetic wound antibacterial applications, ACS Nano 10 (2016) 11000.
[25] J.S. Niu, Y.H. Sun, F.M. Wang, C.Q. Zhao, J.S. Ren, X.G. Qu, Photo modulated nanozyme used for a Gram-selective antimicrobia, Chem. Mater. 30 (2018) 7027.
[26] J.Y. Shan, X. Li, K.L. Yang, W.J. Xiu, Q.R. Wen, Y.Q. Zhang, L.H. Yuwen, L.X. Weng, Z.G. Teng, L.H. Wang, Efficient bacteria killing by Cu_2WS_4 nanocrystals with enzyme-like properties and bacteria-binding ability, ACS Nano 13 (2019) 13797.
[27] L.W. Wang, F.N. Gao, A.Z. Wang, X.Y. Chen, H. Li, X. Zhang, H. Zheng, R. Ji, B. Li, X. Yu, J. Liu, Z.J. Gu, F.L. Chen, C.Y. Chen, Defect-rich adhesive molybdenum disulfide/rGO vertical heterostructures with enhanced nanozyme activity for smart bacterial killing application, Adv. Mater. 32 (2020) 2005423.
[28] W.S. Wang, B.L. Li, H.L. Yang, Z.F. Lin, L.L. Chen, Z. Li, J.Y. Ge, T. Zhang, H. Xia, L. H. Li, Y. Lu, Efficient elimination of multidrug-resistant bacteria using copper sulfide nanozymes anchored to graphene oxide nanosheets, Nano Res. 13 (2020) 2156.
[29] T.M. Chen, H. Zou, X.J. Wu, C.C. Liu, B. Situ, L. Zheng, G.W. Yang, Nanozymatic Antioxidant System Based on MoS_2 Nanosheets, ACS Appl. Mater. Interfaces 10 (2018) 12453.
[30] Z.Z. Wang, K. Dong, Z. Liu, Y. Zhang, Z.W. Chen, H.J. Sun, J.S. Ren, X.G. Qu, Activation of biologically relevant levels of reactive oxygen species by Au/g-C_3N_4 hybrid nanozyme for bacteria killing and wound disinfection, Biomaterials 113 (2017) 145.
[31] H. Wang, P.H. Li, D.Q. Yu, Y. Zhang, Z.Z. Wang, C.Q. Liu, H. Qiu, Z. Liu, J.S. Ren, X. G. Qu, Unraveling the enzymatic activity of oxygenated carbon nanotubes and their application in the treatment of bacterial infections, Nano Lett. 18 (2018) 3344.
[32] J. Fang, H. Wang, X.F. Bao, Y.X. Ni, Y. Teng, J.S. Liu, X.L. Sun, Y. Sun, H.D. Li, Y.M. Zhou, Nanodiamond as efficient peroxidase mimic against periodontal bacterial infection, Carbon 169 (2020) 370.
[33] D.D. Wang, D.L. Jana, Y.L. Zhao, Metal-organic framework derived nanozymes in biomedicine, Acc. Chem. Res. 53 (2020) 1389.
[34] Z.W. Liu, F.M. Wang, J.S. Ren, X.G. Qu, A series of MOF/Ce-based nanozymes with dual enzyme-like activity disrupting biofilms and hindering recolonization of bacteria, Biomaterials 208 (2019) 21.
[35] Y. Zhang, P.P. Sun, L. Zhang, Z.Z. Wang, F.M. Wang, K. Dong, Z. Liu, J.S. Ren, X.G. Qu, Silver-infused porphyrinic metal-organic framework: Surface-adaptive, on-demand nanoplatform for synergistic bacteria killing and wound disinfection, Adv. Funct. Mater. 29 (2019) 1808594.
[36] L.Z. Gao, J. Zhuang, L. Nie, J.B. Zhang, Y. Zhang, N. Gu, T.H. Wang, J. Feng, D.L. Yang, S. Perrett, X. Yan, Intrinsic peroxidase-like activity of ferromagnetic nanoparticles, Nat. Nanotechnol. 2 (2007) 577.
[37] H. Wei, E.K. Wang, Nanomaterials with enzyme-like characteristics (nanozymes): next-generation artificial enzymes, Chem. Soc. Rev. 42 (2013) 6060.
[38] H. Wang, K.W. Wan, X.H. Shi, Recent advances in nanozyme research, Adv. Mater. 31 (2019) 1805368.
[39] L.F. Zhang, L. Zhang, H. Deng, H. Li, W.T. Tang, L.Y. Guan, Y. Qiu, M.J. Donovan, Z. Chen, W.H. Tan, In vivo activation of pH-responsive oxidase-like graphitic nanozymes for selective killing of Helicobacter pylori, Nat. Commun. 2021 (2002) 12.
[40] W.J. Ma, J.J. Mao, X.T. Yang, C. Pan, W.X. Chen, M. Wang, P. Yu, L.Q. Mao, Y.D. Li, A single-atom Fe-N_4 catalytic site mimicking bifunctional antioxidative enzymes for oxidative stress cytoprotection, Chem. Commun. 55 (2018) 159.
[41] J.Z. Li, M.J. Chen, D.A. Cullen, S. Hwang, M.Y. Wang, B.Y. Li, K.X. Liu, S. Karakalos, M. Lucero, H.G. Zhang, C. Lei, H. Xu, G.E. Sterbinsky, Z.X. Feng, D. Su, K.L. More, G.F. Wang, Z.B. Wang, G. Wu, Atomically dispersed manganese catalysts for oxygen reduction in proton-exchange membrane fuel cells, Nat. Catal. 1 (2018) 935.
[42] B.L. Xu, H. Wang, W.W. Wang, L.Z. Gao, S.S. Li, X.T. Pan, H.Y. Wang, H.L. Yang, X. Q. Meng, Q.W. Wu, L.R. Zheng, S.M. Chen, X.H. Shi, K.L. Fan, X.Y. Yan, H.Y. Liu, A single-atom nanozyme for wound disinfection applications, Angew. Chem. Int. Ed. 58 (2019) 4911.
[43] W.W. Wu, L. Huang, E.K. Wang, S.J. Dong, Atomic engineering of single-atom nanozymes for enzyme-like catalysis, Chem. Sci. 11 (2020) 9741.
[44] M.F. Huo, L.Y. Wang, Y.W. Wang, Y. Chen, J.L. Shi, Nanocatalytic tumor therapy by single-atom catalysts, ACS Nano 13 (2019) 2643.
[45] L. Huang, J.X. Chen, L.F. Gan, J. Wang, S.J. Dong, Single-atom nanozymes, Sci. Adv. 5 (2019) eaav5490.
[46] P.P. Qiu, B. Ma, C.T. Hung, W. Li, D.Y. Zhao, Spherical mesoporous materials from single to multilevel architectures, Acc. Chem. Res. 52 (2019) 2928.
[47] X.L. Zhang, G.L. Li, G. Chen, D. Wu, X.X. Zhou, Y.N. Wu, Single-atom nanozymes: A rising star for biosensing and biomedicine, Coordin. Chem. Rev. 418 (2020) 213376.
[48] J. Wei, Z.K. Sun, W. Luo, Y.H. Li, A.A. Elzatahry, A.M. Al-Enizi, Y.H. Deng, D.Y. Zhao, New insight into the synthesis of large-pore ordered mesoporous materials, J. Am. Chem. Soc. 139 (2017) 1706.

[49] G. Wang, S.J. Yang, L. Cao, P.K. Jin, X.K. Zeng, X.W. Zhang, J. Wei, Engineering mesoporous semiconducting metal oxides from metal-organic frameworks for gas sensing, Coordin. Chem. Rev. 445 (2021) 214086.
[50] Q. Xin, H. Shah, A. Nawaz, W.J. Xie, M.Z. Akram, A. Batool, L.Q. Tian, S.U. Jan, R. Boddula, B.D. Guo, Q. Liu, J.R. Gong, Antibacterial carbon-based nanomaterials, Adv. Mater. 31 (2019) 1804838.
[51] S.M. Dong, Y.S. Dong, T. Jia, S.K. Liu, J. Liu, D. Yang, F. He, S.L. Gai, P.P. Yang, J. Lin, GSH-depleted nanozymes with hyperthermia-enhanced dual enzyme-mimic activities for tumor nanocatalytic therapy, Adv. Mater. 32 (2020) 2002439.
[52] J.Y. Shan, K.L. Yang, W.J. Xiu, Q. Qiu, S.L. Dai, L.H. Yuwen, L.X. Weng, Z.G. Teng, L.H. Wang, Cu_2MoS_4 nanozyme with NIR-II light enhanced catalytic activity for efficient eradication of multidrug-resistant bacteria, Small 16 (2020) 2001099.
[53] X.W. Wang, Q.Q. Shi, Z.B. Zha, D.D. Zhu, L.R. Zheng, L.X. Shi, X.W. Wei, L. Lian, K. L. Wu, L. Cheng, Copper single-atom catalysts with photothermal performance and enhanced nanozyme activity for bacteria-infected wound therapy, Bioact. Mater. 6 (2021) 4389.
[54] T. Tsuchido, N. Katsui, A. Takeuchi, M. Takano, I. Shibasaki, Destruction of the outer membrane permeability barrier of Escherichia coli by heat treatment, Appl. Environ. Microb. 50 (1985) 298.
[55] M.C. Wu, A.R. Deokar, J.H. Liao, P.Y. Shih, Y.C. Ling, Graphene-based photothermal agent for rapid and effective killing of bacteria, ACS Nano 7 (2013) 1281.
[56] X. Wei, D. Zheng, M. Zhao, H. Z. Chen, X. Fan, B. Gao, L. Gu, Y. J. B. Guo, Qin, J. Wei, Y. L. Zhao, G. C. Zhang, Cross-linked polyphosphazene hollow nanosphere-derived N/P-doped porous carbon with single nonprecious metal atoms for the oxygen reduction reaction, Angew. Chem. Int. Ed. 2020, 59, 14639.
[57] S.S. Gao, H. Lin, H.X. Zhang, H.L. Yao, Y. Chen, J.L. Shi, Nanocatalytic tumor therapy by biomimetic dual inorganic nanozyme-catalyzed cascade reaction, Adv. Sci. 6 (2019) 1801733.
[58] M.F. Huo, L.Y. Wang, H.X. Zhang, L.L. Zhang, Y. Chen, J.L. Shi, Construction of single-iron-atom nanocatalysts for highly efficient catalytic antibiotics, Small 15 (2019) 1901834.
[59] D.K. Roper, W. Ahn, M. Hoepfner, Microscale heat transfer transduced by surface plasmon resonant gold nanoparticles, J. Phys. Chem. C 111 (2017) 3636.
[60] I. Martinaiou, A.H.A.M. Videla, N. Weidler, M. Kubler, W.D.Z. Wallace, S. Paul, S. Wagner, A. Shahraei, R.W. Stark, S. Specchia, U.I. Kramm, Activity and degradation study of an Fe-N-C catalyst for ORR in Direct Methanol Fuel Cell (DMFC), Appl. Catal. B-Environ. 262 (2020) 118217.
[61] R.C. Mercier, C. Stumpo, M.J. Rybak, Effect of growth phase and pH on the in vitro activity of a new glycopeptide, oritavancin (LY333328), against Staphylococcus aureus and Enterococcus faecium, J. Antimicrob. Chemother. 50 (2002) 19.